Multi-objective optimization of unconventional airfoil at low Reynolds number

Luciana P. Motta[1], Heder S. Bernardino[2], Patrícia H. Hallak[3]

[1]*Graduate Program in Computational Modeling, Federal University of Juiz de Fora, Juiz de Fora, MG, Brazil*
luciana.motta@engenharia.ufjf.br
[2]*Dept. of Computer Science, Federal University of Juiz de Fora, Juiz de Fora, MG, Brazil*
heder@ice.ufjf.br
[3]*Dept. of Applied and Computational Mechanics, Federal University of Juiz de Fora, Juiz de Fora, MG, Brazil*
patricia.hallak@engenharia.ufjf.br

Abstract. The widespread exploration of drones has generated increasing interest in Micro Aerial Vehicles (MAVs). Furthermore, an application that has gained notoriety is the use of aerial vehicles for exploration on Mars. Thus, the quest for efficient aerodynamic profiles for these applications has been intensified. These types of applications operate in a Reynolds number range from 10^4 to 10^5, which is significantly smaller than those commonly found in conventional low Reynolds regimes, such as when commercial drones are adopted. The main objective here is to identify more efficient shapes for airfoils, optimizing them through a multi-objective process aiming to maximize the lift coefficient and minimize the drag coefficient. To achieve this goal, two models of unconventional airfoils were optimized using the Generalized Differential Evolution 3 (GDE3) algorithm. The acquisition of aerodynamic coefficients, essential for evaluating the performance of the evolutionary algorithm, was carried out through simulations using Computational Fluid Dynamics (CFD). The method applied to describe the aerodynamic behavior of the structures proved to be consistent with experimental data. We used as base structur planar model with two inflections. Employing the aircraft's range or autonomy as decision criteria, it was found that the evolutionary algorithm obtained aerodynamic profiles with interesting features for these applications.

Keywords: Unconventional Airfoils, Multi-Objective Optimization, Low-Reynolds Number

1 Introduction

The extensive exploration of Unmanned Aerial Vehicles (UAVs) has generated a significant interest in applications designed for low Reynolds numbers. Notably, there is a growing focus on more aerodynamically challenging scenarios, such as Micro Aerial Vehicles (MAVs) and aerial vehicles designed for planetary exploration, exemplified by Ingenuity, which was sent to Mars. Thus, the quest for efficient aerodynamic profiles for these applications has intensified. These vehicles operate within a Reynolds number range of 10^4 to 10^5, much lower than those typically encountered in conventional low Reynolds regimes, such as those used in commercial drones.

The primary challenge in developing aerial vehicles for these conditions is that the airfoil's boundary layer tends to remain laminar, leading to several issues such as Kelvin-Helmholtz instability, caused by the breakdown of vortices formed at the airfoil's tip, and the Laminar Separation Bubble (LSB), resulting from the lack of boundary layer adhesion [1]. Under these circumstances, conventional airfoils prove inadequate. This inadequacy was demonstrated in wind tunnel tests, where simple flat plates outperformed conventional airfoils for $R_e < 50.000$ [2]. Consequently, there is a pursuit of non-conventional airfoil models that perform better under these conditions. One notable model is the flat plate with two inflections [3].

The inflections in this type of airfoil facilitate the transition from laminar to turbulent flow in the boundary layer, resulting in greater adhesion of this layer. Studying this specific type of airfoil model can directly impact the development of new technologies and improvements to existing devices. The application of multi-objective optimization is valuable for identifying configurations that yield the best results allowing for the selection of the one that best fits the primary objective of each application.

Due to their ability to effectively explore complex, multidimensional search spaces, evolutionary algorithms are ideal for this type of optimization. Given the inherent challenge of finding optimal solutions in low Reynolds number regimes, the capability of evolutionary methods to discover innovative solutions, combined with their

flexibility and robustness, makes them particularly suitable for this application. One algorithm that has proven especially efficient is Generalized Differential Evolution 3 (GDE3). Therefore, the objective of this study is to identify the best configurations for this aerodynamic profile model, using the GDE3 algorithm.

2 Material and Methods

2.1 Airfoil design

In this study, a flat aerofoil with two deflections was optimized, as schematically presented in Figure 1. The parameters used in the model optimization process are x_{le}, δ_{le}, x_{te}, and δ_{te}, which correspond to the position and angle of the leading edge and the position and angle of the trailing edge, respectively. The leading edge of the airfoil is linear, remaining vertical at a zero angle of attack (α).

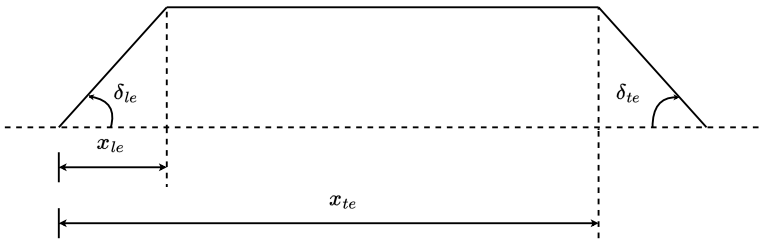

Figure 1. Airfoil shape to be optimized.

The thickness of the airfoil was established as a constant. This choice was guided by the consideration that, for the context in which these airfoils are used, a smaller thickness contributes to more efficient aerodynamics [1]. Thus, the practical feasibility of the project, a fixed thickness equal to 0.8% of the chord was adopted.

2.2 Numerical simulation

Computational modeling was conducted using Computational Fluid Dynamics (CFD) techniques, which is currently the most accurate tool available. Despite the high computational cost of this approach, it is essential for obtaining precise results in the context of unconventional airfoils and low Reynolds number regimes. This necessity arises from the unconventional shape of the airfoil and the complex phenomena involved in such scenarios.

This is applied to solve the Navier-Stokes equation numerically which, in this study, is associated with the Spalart-Allmaras turbulence model. This model proved to be efficient for simulations with low Reynolds numbers, as it can describe the phenomenon of the laminar separation bubble [4]. We implemented this model using OpenFOAM, an open-source software widely recognized in various fields for numerical simulations based on CFD.

The preprocessing tool used for constructing the geometry was Gmsh, which is an open-source software for generating 3D finite element meshes and is integrated with a Computer-Aided Design (CAD) engine. The global mesh size was set to 1 u.c and this value was reduced to 0.01 in the vicinity of the airfoil. The wind tunnel size was 20 u.c in height and 40 u.c in width.

To numerically solve the steady-state Navier-Stokes equation, the Semi-Implicit Method for Pressure Linked Equations (SIMPLE) [5]. This method offers the advantage of handling the coupling between pressure and velocity on the same mesh, thereby mitigating issues arising from strong pressure gradients.

Linear Gauss interpolation was employed for gradients and divergences. The velocity and equivalent-viscosity (nuTilda) divergence terms were resolved using a second-order `linearUpwind` scheme [6] with flux limiter. This scheme utilizes standard upwind interpolations with an explicit correction through the MacCormack predictor-corrector scheme based on the local velocity gradient.

The pressure field (p) was calculated using the numerical method GAMG, an acronym for *Geometric Algebraic MultiGrid*. This method's general principle is to solve the problem in layers, starting with coarse meshes and progressively refining the meshes with each iteration. This allows the algorithm to quickly obtain partial solutions in the upper layers, thereby accelerating the results on refined meshes. The speed gain compared to standard resolution methods depends on the balance between the time savings achieved using coarser meshes and the additional costs of mesh refinement and field data mapping [7].

The velocity field (u) and the turbulent velocity field ($\tilde{u}$) were calculated using the OpenFOAM function `smoothSolver`. To specify the method, it is necessary to indicate the smoother to be used. Given that the Gauss-Seidel method shows good results for pressure-velocity coupling, it was also applied to this resolution.

The tolerance values adopted in the numerical methods used to obtain the fields $\vec{p}$, u, and $\tilde{u}$ were 10^{-6}, 10^{-8}, and 10^{-8}, respectively. The relaxation factor was set to 0.1 for all calculations. The tolerance represents a threshold for the difference between the results of two iterations, indicating the convergence of the equation. On the other hand, the relaxation factor is a constant that determines the intensity of the variation for the next iteration.

2.3 Airfoil optmization

For optimizing the airfoil, it was decided to use an evolutionary algorithm, as these methods are well-suited for problems with complex objective functions. One of the best-known methods in this field is Differential Evolution (DE). Due to its efficiency, DE became the foundation for a series of multi-objective algorithms, among which Generalized Differential Evolution 3 (GDE3) stands out for its particular efficiency. This approach is efficient, can deal with complex search spaces, and demonstrates robustness.

The proposed optimization problem aims to maximize lift and minimize drag coefficients. As the objectives in multi-objective optimization are frequently formulated to be minimized, here we used the minimization of lift multiplied by -1. The formal description of the problem is presented below:

$$\text{Minimize:} \quad f_1(\vec{x}), f_2(\vec{x}) = \begin{cases} -C_{l_{mean}}, C_{d_{mean}} & \text{if } |C_{d_{mean}}| < 100, \\ 100, 100 & \text{otherwise.} \end{cases} \tag{1}$$

where $C_{l_{\text{mean}}}$ and $C_{d_{\text{mean}}}$ are the average values of the lift and drag coefficients, respectively, for a structure generated by $\vec{x}$. These coefficients are determined through the average of the values obtained when the angle of attack is varied from 0° to 12°, with increments of 3°. Each point within this interval requires a simulation in OpenFOAM. Thus, limiting the range to 12° and the application of the static penalty aims to reduce the chances of conducting simulations with angles that could lead to stall, given a significant increase in computational cost of the simulation.

3 Computational Experiments

In this section, we present the validation of the model used to generate data throughout the optimization process, as well as the results obtained from the optimization. During the validation phase, the simulation data was compared with wind tunnel test data. For the optimization phase, we employed the GDE3 algorithm in conjunction with simulations in OpenFOAM, presenting the results in terms of range and endurance. The code and supplementary material can be accessed at: GitHub repository GDE3_twoBendsAirfoil.

3.1 Model validation

To demonstrate the model's fidelity, a comparison will be made between the computational simulation results and experimental data from wind tunnel tests. This process evaluates the validity of using the simulation for optimization. In low Reynolds number regimes, model variations cause more pronounced aerodynamic changes. This sensitivity impacts simulations and the experimental phase in wind tunnels, where considerable variations in independent measurements can occur within the specific range considered for this work [8].

Consequently, it is essential that the data come from a single source with many samples and low variation between independent measurements. Thus, data were taken from Traub and Coffman [3], which provides a large amount of consistent experimental data. They used equipment with a precision of 0.05 degrees for the angle of attack. To analyze the reproducibility between independent measurements, a cambered airfoil with a span of 304.8 mm and $R_e = 4 \times 10^4$ was used, resulting in C_l between 0.2% and 0.32%, with a confidence interval of 99%.

For validating the computational model, four distinct sets of instances were used. The first and second sets involve varying the Reynolds number: the first for a simple flat airfoil, chosen for its simplicity, and the second for an airfoil with good aerodynamic performance, chosen for contrast. Sets three and four consist of experiments with fixed Reynolds numbers but vary the angles of the leading edge and trailing edge deflection, respectively.

The initial set of instances involves varying only the Reynolds number for a simple flat plate. The absolute error of the angle of attack for C_l and C_d is shown in Figure 2. As noted, the model accurately replicates the behavior of the aerodynamic coefficients, including the range of negative angles of attack and the section following the stall point. The disparities between the errors for each Reynolds number are insignificant in this case.

The second set of instances involves varying the Reynolds number applied to an airfoil with the following design variable values: $x_{le} = 0.1$, $\delta_{le} = 15$, $x_{te} = 0.8$, and $\delta_{te} = 15$. The absolute error concerning the angle of attack for C_l and C_d is shown in the graphs presented in Figure 3, respectively. A larger error can be noted compared to the previous set of instances. This occurs due to the increased turbulence introduced by airfoils with

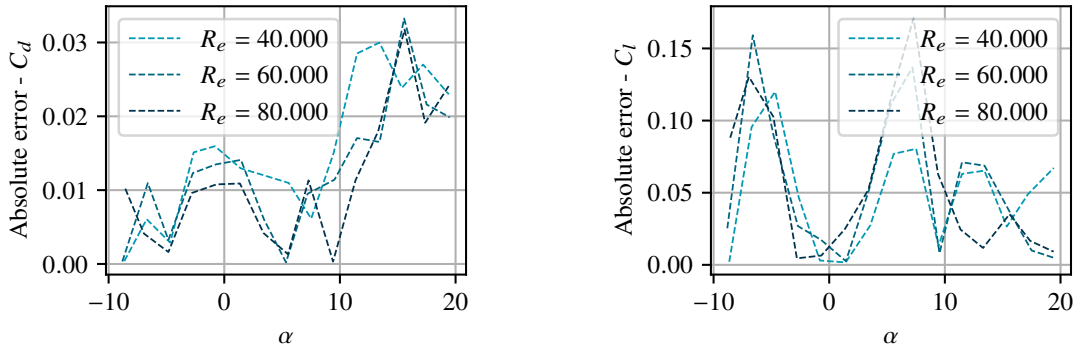

Figure 2. Error in aerodynamic coefficients (C_d on the left and C_l on the right) relative to Reynolds number for the flat plate.

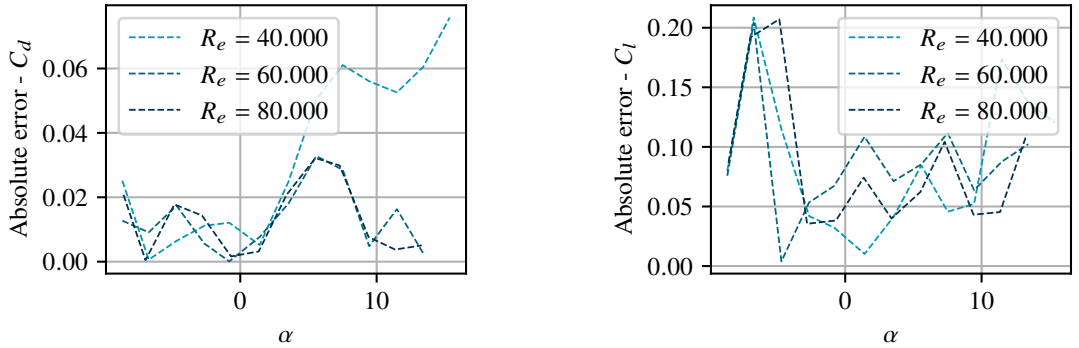

Figure 3. Error in aerodynamic coefficients (C_d at left and C_l at right) relative to Reynolds number for the set of the baseline model.

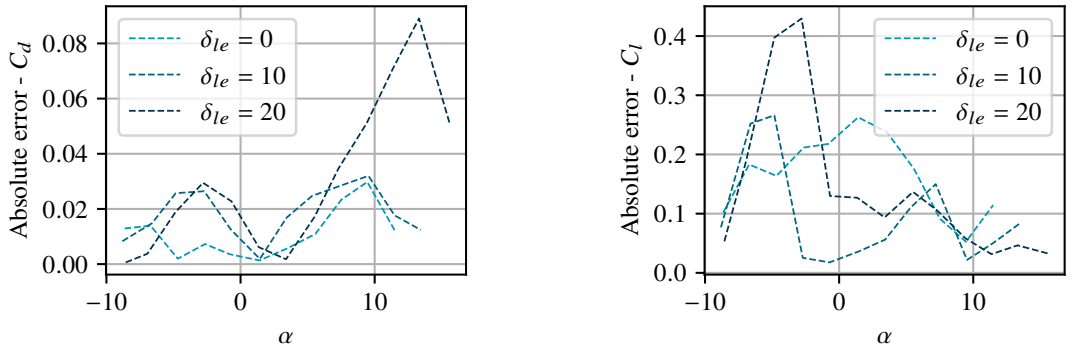

Figure 4. Error in aerodynamic coefficients (C_d on the left and C_l on the right) relative to Reynolds number for the set with modification at the leading edge.

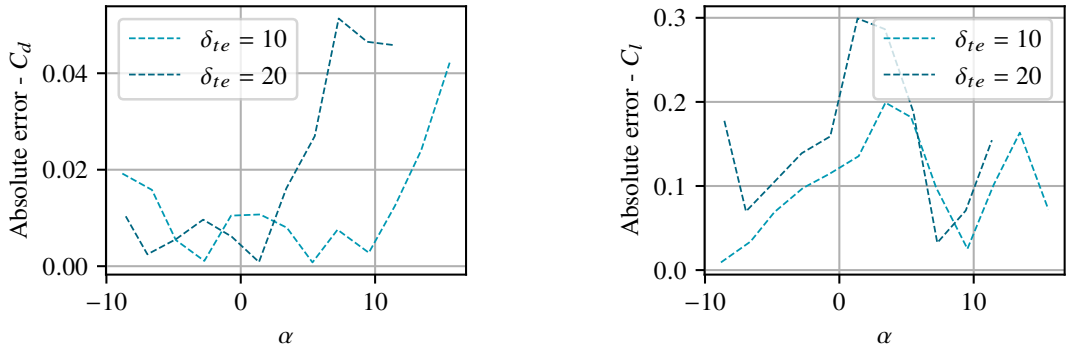

Figure 5. Error in aerodynamic coefficients (C_d on the left and C_l on the right) relative to Reynolds number for the set with modification at the trailing edge.

deflections. While this is a desirable effect for the airfoil's aerodynamics, it can add greater complexity to the simulation. However, the model still satisfactorily reproduces the behavior of the aerodynamic coefficients, with a more pronounced discrepancy for negative angles of attack and angles of attack beyond the stall point. It is important to highlight that the higher error for the instance with Re = 40.000 is expected, as the challenges related to low Reynolds number conditions increase rapidly with the decrease of this parameter.

The next set of instances maintains the same configuration as the previous case for the trailing edge, i.e., $x_{te} = 0.8$ and $\delta_{te} = 15^{\circ}$. However, a modification was implemented in the position of the leading edge, now defined as $x_{le} = 0.2$. In this set, the Reynolds number was kept constant at $Re = 60.000$, but the leading edge angle was individually adjusted for each element. The absolute error concerning the angle of attack for C_l and C_d is shown in the graphs presented in Figure 4, respectively. In this context, a clear trend of improvement is notable regarding the model's fit to the data for smaller angles.

The final set of instances aims to evaluate the influence of the alteration in the trailing edge of the airfoil on the model's quality. In this case, the airfoil is maintained only with the rear bend. Therefore, the leading edge angle is adjusted to be equal to the angle of the tangent generated by the height of the rear bend at its position on the x-axis (x_{te}). As in the previous case, the Reynolds number was kept constant at $Re = 60.000$. The absolute error concerning the angle of attack for C_l and C_d is shown in the graphs presented in Figure 4, respectively. The result was similar to the previous case: the smaller the trailing edge angle, the smaller the error found for the model.

As observed, the decrease in the Reynolds number and the increase in the angles of the leading and trailing edges generate a more pronounced discrepancy concerning the data obtained from wind tunnel tests. However, the errors remained acceptable for all instances and were more pronounced only for negative angles of attack and for angles of attack beyond the stall point. This effect was expected due to the instability present in these ranges. To avoid carrying these larger errors into the optimization process, the angle of attack considered for the calculation of the mean aerodynamic coefficients was limited to a safer range.

3.2 Analysis of optimization results

In order to analyze the obtained results, the airfoils indicated for maximum endurance and maximum range for each Reynolds number were examined, taken from the Pareto curve resulting from the set of the 10 Pareto curves from the optimization processes. These two objectives were selected because they are essential for the energy efficiency of aerial vehicles. Given that in low Reynolds number applications the total weight of the aerial vehicle is a crucial factor, reducing energy consumption, and thus reducing the number or capacity of the batteries, is essential for the viability of these vehicles. Therefore, the analysis was focused on the following airfoils:

1. **Aerofoil for maximum autonomy**: The autonomy of an aerial vehicle is the amount of time it can remain in flight with a given amount of fuel, and a well-known function to evaluate the autonomy of a airfoil is $f_{d_1} = C_l/C_d$.
2. **Aerofoil for maximum range:** The range of an aerial vehicle is the distance that it can fly with a given amount of fuel, and a well-known function to evaluate the range of a airfoil is $f_{d_2} = C_l^3/C_d^2$.

The airfoils for maximum autonomy and maximum range are presented in Figure 6f and 6f, respectively. The exact values of the design variables and the average values of the aerodynamic coefficients, for each case, are described in Table 1. The averages are the same as those used in the objective functions during the optimization phase, with the mean values for C_d and C_l taken for angles of attack ranging from 0° to 12°, in 3° intervals.

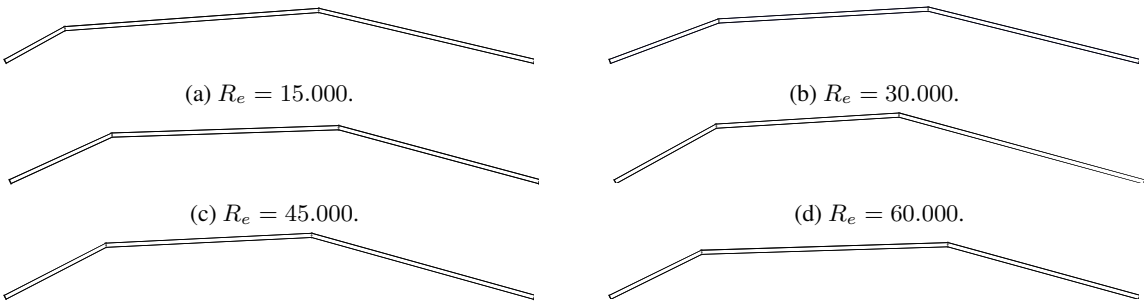

(a) $R_e = 15.000$. (b) $R_e = 30.000$.

(c) $R_e = 45.000$. (d) $R_e = 60.000$.

(e) $R_e = 75.000$. (f) $R_e = 90.000$.

Figure 6. Projects optimized by Reynolds number - C_l/C_d

To analyze the efficiency of the obtained results, a comparison was made between a model that proved to be aerodynamically efficient for low Reynolds number conditions [3] and the model obtained through the optimization process proposed in this work, for $R_e = 60,000$. The airfoil used as the comparison baseline is the flat airfoil with

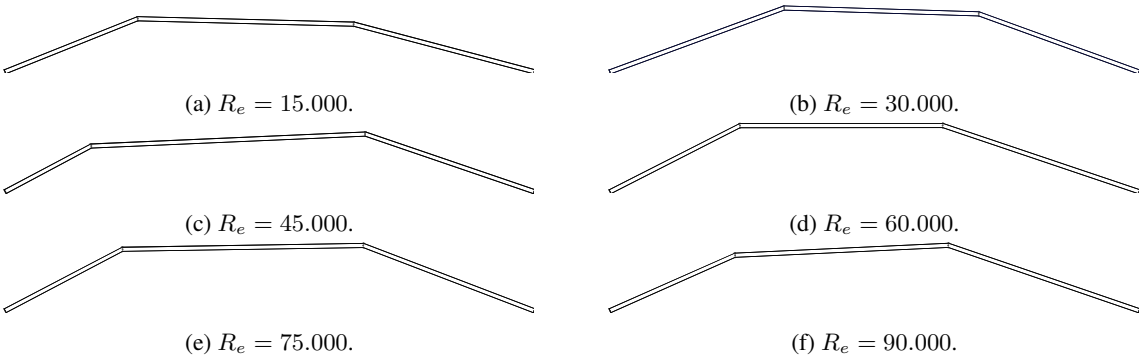

(a) $R_e = 15.000$. (b) $R_e = 30.000$. (c) $R_e = 45.000$. (d) $R_e = 60.000$. (e) $R_e = 75.000$. (f) $R_e = 90.000$.

Figure 7. Projects optimized by Reynolds number - C_l^3/C_d^2

Table 1. Description of projects optimized by Reynolds number (R_e).

	Autonomy						Range					
R_e	x_{le}	δ_{le}	x_{te}	δ_{te}	C_d médio	C_l médio	x_{le}	δ_{le}	x_{te}	δ_{te}	C_d médio	C_l médio
15.000	0.12549	28.75°	0.59214	13.29°	0.13628	1.26193	0.26192	15.01°	0.65754	14.77°	0.14238	1.31616
30.000	0.21399	20.38°	0.59947	13.90°	0.12782	1.31285	0.33713	20.13°	0.69025	19.89°	0.14778	1.45512
45.000	0.20508	24.56°	0.61964	15.04°	0.12768	1.38715	0.17721	27.94°	0.67518	18.82°	0.13634	1.45476
60.000	0.20910	28.77°	0.53966	15.19°	0.13009	1.45151	0.26220	26.95°	0.62681	18.62°	0.13840	1.52853
75.000	0.20662	27.27°	0.57982	15.54°	0.12293	1.42822	0.23833	27.64°	0.67112	20.91°	0.13504	1.54689
90.000	0.18675	26.18°	0.63655	15.35°	0.12280	1.42113	0.24813	23.91°	0.63436	18.91°	0.13328	1.53106

two deflections, which has the following design variable values: $x_{le} = 0.1$, $\delta_{le} = 15°$, $x_{te} = 0.8$, and $\delta_{te} = 15°$.

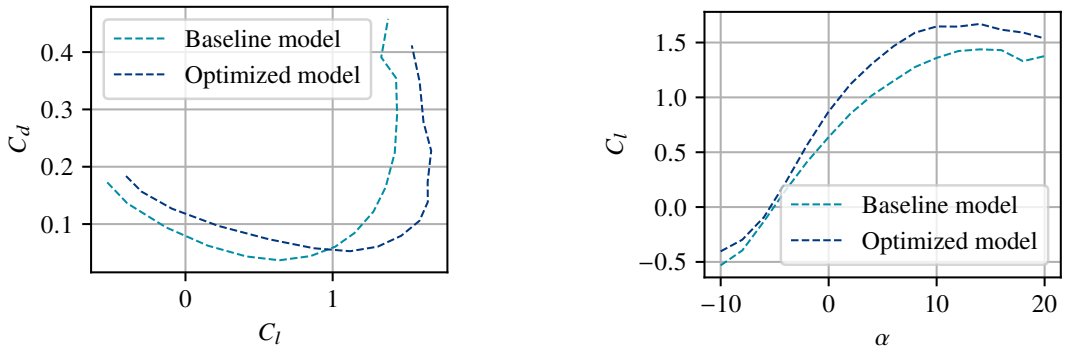

(a) $C_l \times C_d$. (b) $\alpha \times C_l$.

Figure 8. Plots comparing the performances of the optimized model and baseline model - autonomy.

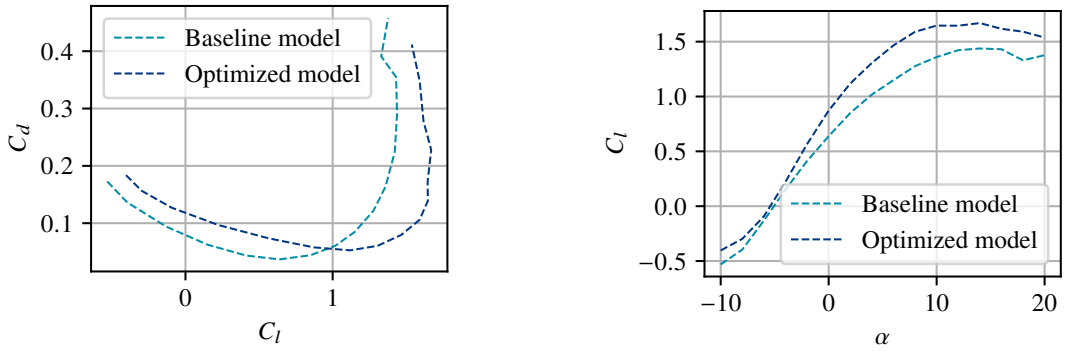

(a) $C_l \times C_d$. (b) $\alpha \times C_l$.

Figure 9. Comparative graphs of the performance between the optimized model and the baseline model - range.

Applying the C_l/C_d function to the literature model yields a value of 10.13, while the model selected in this study achieves a value of 11.16. This indicates a significant improvement in the autonomy of the aerial vehicle with the optimization process. Applying the C_l^3/C_d^2 function to the literature model yields a value of 112.67, while the model selected in this study achieves a value of 186.44. This indicates a significant improvement in the range of the aerial vehicle with the optimization process.

4 Conclusions

In this work, we search for efficient aerodynamic profiles in low Reynolds number regimes using GDE3, a multi-objective approach. To achieve this goal, CFD computational modeling was performed to simulate the candidate solutions, providing the average values of C_d and C_l, which were used in the evaluation function. Also, the model's fidelity to experimental data was demonstrated, validating the simulation for evaluating the solutions.

The initial results presented included comparisons between the computationally generated data and wind tunnel experiment data. As demonstrated, the simulation was generally able to reproduce the behavior of the aerodynamic coefficients, showing small average errors. A more significant variation was observed for the negative angles of attack or above the stall point. Therefore, the results indicate that the model chosen for the simulation is a reliable source for generating the data used to evaluate the solutions during the optimization process.

The results obtained in the optimization stage for airfoils for maximum autonomy and maximum range were presented. In addition, comparisons were performed between the airfoils obtained through the optimization process and an airfoil from the literature known for its aerodynamic efficiency. As shown, the optimized airfoils presented a high lift coefficient, with minimal loss in drag coefficient when compared to the known efficient model. A significant advantage in terms of autonomy and range was also observed.

For future work, we suggest a comprehensive mesh convergence study, exploring the sensitivity of the solution to different discretizations. Also, including the moment coefficient among the evaluation criteria (lift and drag) can yield interesting results and enhance the optimization process. The use of an adaptive penalty technique can provide flexibility to the algorithm, potentially resulting in better solutions.

Acknowledgements. The authors thank the financial support provided by CNPq, CAPES, FAPEMIG, and UFJF.

Authorship statement. The authors hereby confirm that they are the sole liable persons responsible for the authorship of this work, and that all material that has been herein included as part of the present paper is either the property (and authorship) of the authors, or has the permission of the owners to be included here.

References

[1] W. J. Koning, E. A. Romander, and W. Johnson. *Optimization of low Reynolds number airfoils for martian rotor applications using an evolutionary algorithm*, pp. 0084. AIAA, 2020.

[2] E. Laitone. Wind tunnel tests of wings at reynolds numbers below 70 000. *Experiments in fluids*, vol. 23, n. 5, pp. 405–409, 1997.

[3] L. W. Traub and C. Coffman. Efficient low-reynolds-number airfoils. *Journal of Aircraft*, vol. 56, n. 5, pp. 1987–2003, 2019.

[4] P. Spalart and S. Allmaras. *A one-equation turbulence model for aerodynamic flows*, pp. 439. AIAA, 1992.

[5] S. V. Patankar and D. B. Spalding. A calculation procedure for heat, mass and momentum transfer in three-dimensional parabolic flows. *Numerical prediction of flow, heat transfer, turbulence and combustion*, vol. 1, pp. 54–73, 1983.

[6] R. F. Warming and R. M. Beam. Upwind second-order difference schemes and applications in aerodynamic flows. *AIAA Journal*, vol. 14, n. 9, pp. 1241–1249, 1976.

[7] CFD Direct. User guide openfoam, v11 - `fvSolution`. `https://doc.cfd.direct/openfoam/user-guide-v11/fvsolution`. Accessed: 2024-07-10, 2023.

[8] J. Winslow, H. Otsuka, B. Govindarajan, and I. Chopra. Basic understanding of airfoil characteristics at low reynolds numbers (10 4–10 5). *Journal of aircraft*, vol. 55, n. 3, pp. 1050–1061, 2018.